



Article

Second-Order Central Difference Particle Filter Algorithm for State of Charge Estimation in Lithium-Ion Batteries

Yuan Chen and Xiaohe Huang *

School of Artificial Intelligence, Anhui University, Hefei 230093, China; cumtjiangsucusy@126.com

* Correspondence: wa22301103@stu.ahu.edu.cn

Abstract: The estimation of the state of charge (SOC) in lithium-ion batteries is a crucial aspect of battery management systems, serving as a key indicator of the remaining available capacity. However, the inherent process and measurement noises created during battery operation pose significant challenges to the accuracy of SOC estimation. These noises can lead to inaccuracies and uncertainties in assessing the battery's condition, potentially affecting its overall performance and lifespan. To address this problem, we propose a second-order central difference particle filter (SCDPF) method. This method leverages the latest observation data to enhance the accuracy and noise adaptability of SOC estimation. By employing an improved importance density function, we generate optimized particles that better represent the battery's dynamic behavior. To validate the effectiveness of our proposed algorithm, we conducted comprehensive comparisons at both 25 °C and 0 °C under the new European driving cycle condition. The results demonstrate that the SCDPF algorithm exhibits a high accuracy and rapid convergence speed, with a maximum error which never exceeds 1.30%. Additionally, we compared the SOC estimations with both Gaussian and non-Gaussian noise to assess the robustness of our proposed algorithm. Overall, this study presents a novel approach to enhancing SOC estimation in lithium-ion batteries, addressing the challenges posed by the process itself and measurement noises.

Keywords: state of charge; battery management system; second-order central difference particle filter; importance density function



Citation: Chen, Y.; Huang, X.

Second-Order Central Difference Particle Filter Algorithm for State of Charge Estimation in Lithium-Ion Batteries. *World Electr. Veh. J.* **2024**, *15*, 152. <https://doi.org/10.3390/wevj15040152>

Academic Editor: Peter Van den Bossche

Received: 18 March 2024

Revised: 1 April 2024

Accepted: 4 April 2024

Published: 7 April 2024



Copyright: © 2024 by the authors. Licensee MDPI, Basel, Switzerland. This article is an open access article distributed under the terms and conditions of the Creative Commons Attribution (CC BY) license (<https://creativecommons.org/licenses/by/4.0/>).

1. Introduction

Lithium-ion batteries are rapidly becoming the first choice for pure electric or hybrid electric vehicles, satellites, and aircraft because of their advantages of high energy density and power endurance, high nominal voltage, low self-discharge rate, long cycle, and no memory effect [1,2]. Nickel–manganese–cobalt oxide batteries, which have a high energy density and can provide a large amount of energy in a short time, have become a major development trend for lithium-ion batteries.

Accurate state of charge (SOC) estimation can improve the mileage per charge of electric vehicles and help users to formulate reasonable travel plans to ensure the normal operation of their electric vehicles [3]. However, it cannot be directly measured in practical situations and needs to be calculated using battery voltage, current, and temperature [4]. Accurately tracking the trajectory of the actual battery SOC is an unsolved problem due to the time-varying and nonlinear characteristics of the battery SOC. Various SOC estimation methods exist including the open circuit voltage [5], ampere-hour integral [6], Kalman filter (KF) [7–10], and particle filter (PF) [11–14]. In recent years, data-driven estimation methods such as artificial neural networks [15–17] and support vector machines [18,19] have also been applied to the research of SOC estimation. Model-based filter methods are promising for real SOC estimation applications due to their high accuracy and robustness. In recent years, electrochemical model-based techniques have been widely investigated because they can provide more valuable and essential information [20,21]. However, the electrochemical

model is complex and requires a large number of calculations, which is unsuitable for online real-time applications. The most commonly used models are equivalent circuit models [22,23]. A second-order RC network model is the most common one which shows good balance between accuracy and complexity. Battery model accuracy is also affected by the model parameter identification algorithm. The identification algorithms include the pulse current [24], recursive least square (RLS) [25–27], particle swarm optimization [28,29], and so on [30–32]. The most commonly used method is the RLS and its subsequent improvement, and the forgetting factor RLS (FFRLS) is an ideal identification algorithm for second-order RC models because of its comprehensive performance [33].

KF is an optimized processing method applied to discrete random systems, and it was proposed by the famous scholar Kalman in 1960 [34]. Improved KF methods such as extended KF (EKF) [35] and sigma point KF [36] have good dynamic characteristics, a high estimation accuracy, and require a moderate number of calculations because they can solve the problems caused by nonlinear systems and first-order Taylor expansion. Wang et al. [37] emphasized the limitations of the EKF caused by battery parameter variations. They proposed a second-order RC model calibrated through offline testing. The impact of open circuit voltage (OCV) deviation on EKF-estimated SOC accuracy was quantified, and a Dynamic Matrix Control-based model parameter-updating method was introduced to enhance parameter accuracy, thereby improving SOC precision. Zhou et al. [38] proposed a novel variational EKF technique to enhance SOC estimation accuracy for batteries. They utilized a second-order equivalent circuit model and incorporated a least square error method. By addressing resistance polarization during SOC decrease, they dynamically adjusted system parameters online. Introducing the variation theorem facilitated the real-time tracking of system parameters. Experimental comparisons demonstrated the superiority of the variational EKF over traditional EKF methods in terms of accuracy and robustness, validating the efficacy of the proposed approach. Maheshwari et al. [39] employed the EKF for real-time SOC estimation. However, the sensitivity of this model to noise covariance matrices was observed. To address this issue, they applied the Sunflower Optimization algorithm (SFO) to optimize these matrices prior to EKF implementation, ensuring accuracy and mitigating divergence. An evaluation covering various methodologies showcased its superior accuracy and convergence, even under conditions of an initially inaccurate SOC. Wang et al. [40] proposed an adaptive robust unscented Kalman filter (ARUKF) for accurate and adaptable SOC estimation. The approach integrates a DP battery model for dynamic behavior emulation, employing online parameter identification via the improved forgetting factor recursive least squares (IFFRLS) method. Additionally, the Institute of Geodesy and Geophysics' (IGGIII) weight function enhances the robustness of UKF, adjusting the observation residuals' weights. Receding horizon-based adaptive filter tuning refines time-varying noise covariance. Joint estimation of the battery's model parameters and SOC with capacity updating mitigates system disturbances, which has been verified through cycle and aging tests showcasing its superior accuracy and convergence. Traditional UKF struggles with unknown or inaccurate noise statistics, resulting in suboptimal SOC estimation due to non-positive error covariance. Xing et al. [41] introduced an Improved Adaptive Unscented Kalman Filter (IAUKF) comprising an Improved UKF (IUKF) and a Sage–Husa adaptive filter to address this issue by stabilizing estimation and adapting noise statistics. Experimental validation against the federal urban driving schedule demonstrates IAUKF's superior accuracy and stability compared to IUKF and UKF, affirming its effectiveness. However, the system process and measurement noise within the methods should be independent Gaussian white noise; otherwise, the filtering may diverge.

The PF algorithm, as a statistical filtering method, can overcome the shortcomings of the KF methods with non-Gaussian noise and has a higher estimation accuracy and more flexibility and applicability. Chen et al. [42] proposed a universal battery model based on differential voltage analysis with EKF and PF methods for SOC estimation. The results show that a higher estimation accuracy can be achieved. In Monte Carlo sampling, an error exists in the method of approximately selecting a prior probability density as an

important density function. The particles will degenerate with the increase in the number of iterations. Choosing a reasonable importance density function and carrying out resampling can address the particle degeneracy phenomenon [43,44]. Xu et al. [45] proposed a new method to solve the particle shortage by using the UKF to generate the importance density function and the PSO to improve the resampling process. A weight-selection PF algorithm is proposed in [46] for SOC estimation to solve the particle degradation problem within PF. The algorithm had a high estimation accuracy and good robustness under hybrid pulse power characteristic (HPPC) test and DST experiment verification. Hao et al. [47] enhanced the accuracy of the FFRLS method by employing a particle swarm optimization algorithm to select the parameter's optimal initial values and forgetting factor values. They further integrated the UKF into the PF as the density function, forming the Unscented Particle Filter (UPF) algorithm. Computational results that were gathered under various conditions demonstrated the algorithm's strong convergence and high system robustness. Wang et al. [48] proposed a SOC estimation method called the Grey Wolf Optimization Particle Filter (GWO-PF). The GWO-PF method integrates particle distribution mechanisms with Grey Wolf Optimization, utilizing a second-order battery equivalent circuit model and recursive least squares with a forgetting factor to achieve an accurate SOC estimation.

In this study, a new second-order central difference PF (SCDPF) algorithm is applied for accurate SOC estimation. First, a second-order central difference KF (SCDKF) is used as an importance density function to generate optimized particles to overcome the particle degeneracy problem of the PF. Then, an error comparison and convergence analysis are conducted for different battery SOC estimation algorithms under the new European driving cycle (NEDC) conditions at different temperatures to verify the accuracy and real-time performance of the proposed algorithm. Finally, Gaussian and non-Gaussian noises are added to battery current and voltage to analyze the robustness of the proposed algorithm.

This paper exhibits several innovative and advantageous aspects, including the following:

1. **An Innovative Algorithm:** We apply the SCDPF algorithm to lithium battery SOC estimation for the first time. In contrast to traditional particle filtering (PF) methods, the SCDPF algorithm utilizes Second-order Central Difference Kalman Filtering (SCDKF) as the importance density function to generate optimized particles, effectively addressing the particle degeneracy issue inherent in traditional PF approaches.
2. **Accuracy Enhancement:** By employing improved importance density functions and central difference methods, the SCDPF algorithm significantly enhances SOC estimation accuracy.
3. **Robustness Enhancement:** We incorporate the handling of Gaussian and non-Gaussian noise within the algorithm, verifying its robustness by introducing noise into the battery current and voltage signals. The results indicate that the SCDPF algorithm maintains a high estimation accuracy under the influence of noise, particularly demonstrating a better robustness than existing methods under non-Gaussian noise conditions.
4. **Experimental Validation:** Experimental validation is conducted under different temperature conditions, including 25 °C and 0 °C, demonstrating not only the effectiveness of the algorithm but also its applicability and stability under various temperature conditions.

The remainder of the paper is organized as follows. Section 2 describes the establishment of the battery model and the parameter identification. Section 3 introduces the PF and SCDPF algorithms. Section 4 conducts the experiment and simulation analysis. Our conclusions are summarized in Section 5.

2. Battery Model and Parameter Identification

2.1. Equivalent Circuit Model of Second-Order RC

Figure 1 shows the second-order RC equivalent circuit.

R_{ac} is the Ohmic resistance, R_{ct} is the charge transfer resistance which represents the electrochemical polarization effect, and R_{wb} is the diffusion resistance which represents the

concentration polarization effect. C_{ct} and C_{wb} represent the charge transfer capacitance and diffusion capacitance, respectively. U_{ocv} and U_t represent the open circuit voltage and the output voltage, respectively.

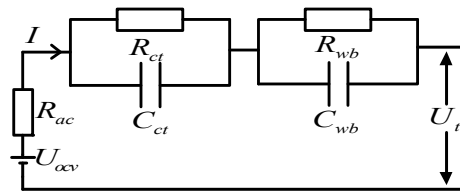


Figure 1. Equivalent circuit model of second-order RC.

The electrical equation can be obtained using Equation (1):

$$\begin{aligned} \dot{U}_{ct} &= \frac{1}{C_{ct}} I(t) - \frac{1}{C_{ct}R_{ct}} U_{ct} \\ \dot{U}_{wb} &= \frac{1}{C_{wb}} I(t) - \frac{1}{C_{wb}R_{wb}} U_{wb} \\ U_t &= U_{ocv} - U_{ct} - U_{wb} - R_{ac}I(t), \end{aligned} \tag{1}$$

where \dot{U}_{ct} is the derivative of U_{ct} , \dot{U}_{wb} is the derivative of U_{wb} , U_{ct} is the terminal voltage of R_{ct} , and U_{wb} is the terminal voltage of R_{wb} .

By discretizing Equation (1), the state-space equation of the battery can be obtained as

$$x_k = f(x_{k-1}) = A_{k-1} \cdot x_{k-1} + B_{k-1} \cdot I_{k-1} + \omega_{k-1} \tag{2}$$

where $A_{k-1} = \begin{bmatrix} 1 & 0 & 0 \\ 0 & e^{-\frac{\Delta t}{\tau_{ct}}} & 0 \\ 0 & 0 & e^{-\frac{\Delta t}{\tau_{wb}}} \end{bmatrix}$, $B_{k-1} = \begin{bmatrix} -\frac{\Delta t}{C} \\ R_{ct} \cdot \left(1 - e^{-\frac{\Delta t}{\tau_{ct}}}\right) \\ R_{wb} \cdot \left(1 - e^{-\frac{\Delta t}{\tau_{wb}}}\right) \end{bmatrix}$, $x_k = [SOC(k); U_{ct}(k); U_{wb}(k)]$.

Δt is the sampling interval, and k is the sampling moment. ω_k is the process' Gaussian white noise, which is mainly caused by system noise and model error. τ_{ct} is the time constant of $R_{ct}C_{ct}$, and τ_{wb} is the time constant of $R_{wb}C_{wb}$. $\tau_{ct} = R_{ct} \times C_{ct}$, $\tau_{wb} = R_{wb} \times C_{wb}$.

The terminal voltage prediction equation for the battery model is given as follows:

$$y_k = h(x_k) = C_k \cdot x_k + D_k \cdot I_k + v_k \tag{3}$$

where $C_k = [\frac{\partial U_{ocv}}{\partial SOC} \quad -1 \quad -1]$, $D_k = -R_{ac}$, and v_k is the Gaussian white noise, which is mainly caused by experimental measurement equipment. y_k is the terminal voltage of battery model at k .

2.2. Parameter Identification of Battery Model

In this study, the FFRLS algorithm is employed for parameter identification. The model is written in least square form as follows, as has been elaborated upon in the literature:

$$y(k) = \phi(k)\theta^T + e(k) \tag{4}$$

where $\phi(k) = [y_{k-1}, y_{k-2}, I_k, I_{k-1}, I_{k-2}]$, $e(k)$ is the sensor sampling error at k , and the parameter matrix $\theta = [\theta_1, \theta_2, \theta_3, \theta_4, \theta_5]$.

The formulas for the FFRLS algorithm are described as follows:

$$\begin{cases} \hat{\theta}(k) = \hat{\theta}(k-1) + K(k)[y(k) - \phi^T(k)\hat{\theta}(k-1)] \\ K(k) = P(k-1)\phi(k)[\lambda + \phi^T(k)P(k-1)\phi(k)]^{-1} \\ P(k) = \frac{1}{\lambda}[I - K(k)\phi^T(k)]P(k-1) \end{cases} \tag{5}$$

where $\theta(k - 1)$ is the estimated values of parameters at moment $k - 1$, $\varphi^T(k)\theta(k - 1)$ is the observations made in the current moment, and λ is the forgetting factor with a value of 0.98.

3. SOC Estimation Algorithm Based on Improved PF

The SCDPF is an optimized PF method for SOC estimation which has a higher precision than the PF and the UPF methods [49]. It uses an SCDKF as an important density function to generate optimized particles to reduce the deviation between the sample and the actual sample. The Stirling interpolation formula is used for nonlinear approximation in the form of central difference, which leads to higher accuracy than that of the second-order Taylor expansion. The computational complexity is low because the Jacobian matrix of the system's function does not need to be calculated. The square root form of the covariance matrix is used to ensure the positive definiteness of the covariance matrix, and the filtering performance is better than that of the UKF algorithm.

The Stirling interpolation formula is shown below.

$$y \approx f(\bar{x}) + \bar{D}_{\nabla_x} f(\bar{x})(x - \bar{x}) + \frac{1}{2!} \bar{D}_{\nabla_x}^2 f(\bar{x})(x - \bar{x})^2 \quad (6)$$

where \bar{D}_{∇_x} is the first-order central difference operator, $\bar{D}_{\nabla_x} f(\bar{x}) = \frac{1}{\lambda} [f(\bar{x} + \lambda) - f(\bar{x})]$. $\bar{D}_{\nabla_x}^2$ is the second-order central difference, $\bar{D}_{\nabla_x}^2 f(\bar{x}) = \frac{1}{\lambda^2} [f(\bar{x} + \lambda) + f(\bar{x} - \lambda) - 2f(\bar{x})]$. λ is the given step size with a value of $\lambda^2 = 3$.

The procedures of SCDKF are elaborated as follows:

1. Initialization: By using Cholesky decomposition, some operators are calculated using the following equation:

$$P_{pc} = S_{xp} \times S_{xp}^T, P_{ec} = S_{xe} \times S_{xe}^T, Q = S_v \times S_v^T, R = S_w \times S_w^T \quad (7)$$

where P_{pc} and P_{ec} represent the prediction and estimated covariance, respectively, which are constantly updating. Q represents the process noise covariance matrix, and R represents the measuring noise covariance matrix. S_{xp} represents the square root decomposition operator of P_{pc} , and S_{xe} represents the square root decomposition operator of P_{ec} . S_v represents the square root decomposition operator of Q . S_w represents the square root decomposition operator of R .

The matrix that is required can be obtained from Equations (8) and (9).

$$\begin{aligned} (S_{xx}^{(1)}(i))^{(k)} &= \alpha(f(x_{i-1}^{(k)} + \lambda S_{xe,l}, \omega_{i-1}) - f(x_{i-1}^{(k)} - \lambda S_{xe,l}, \omega_{i-1})); l = 1 : m_x \\ (S_{xv}^{(1)}(i))^{(k)} &= \alpha(f(x_{i-1}^{(k)}, \omega_{i-1} + \lambda S_{v,l}) - f(x_{i-1}^{(k)}, \omega_{i-1} - \lambda S_{v,l})); l = 1 : m_x \\ (S_{y_{px}}^{(1)}(i))^{(k)} &= \alpha(h(x_{pi}^{(k)} + \lambda S_{xp,l}, v_i) - h(x_{pi}^{(k)} - \lambda S_{xp,l}, v_i)); l = 1 : m_x \\ (S_{yw}^{(1)}(i))^{(k)} &= \alpha(h(x_{pi}^{(k)}, v_i + \lambda S_{w,l}) - h(x_{pk}^{(k)}, v_i - \lambda S_{w,l})); l = 1 : m_v \end{aligned} \quad (8)$$

$$\begin{aligned} (S_{xx}^{(2)}(i))^{(k)} &= \beta(f(x_{i-1}^{(k)} + \lambda S_{xe,l}, \omega_{i-1}) + f(x_{i-1}^{(k)} - \lambda S_{xe,l}, \omega_{i-1}) - 2f(x_{i-1}^{(k)}, \omega_{i-1})); \\ (S_{xv}^{(2)}(i))^{(k)} &= \beta(f(x_{i-1}^{(k)}, \omega_{i-1} + \lambda S_{v,l}) + f(x_{i-1}^{(k)}, \omega_{i-1} - \lambda S_{v,l}) - 2f(x_{i-1}^{(k)}, \omega_{i-1})); \\ (S_{y_{px}}^{(2)}(i))^{(k)} &= \beta(h(x_{pi}^{(k)} + \lambda S_{xp,l}, v_i) + h(x_{pi}^{(k)}, v_i - \lambda S_{xp,l}) - 2h(x_{pi}^{(k)}, v_i)); \\ (S_{yw}^{(2)}(i))^{(k)} &= \beta(h(x_{pi}^{(k)}, v_i + \lambda S_{w,l}) + h(x_{pi}^{(k)}, v_i - \lambda S_{w,l}) - 2h(x_{pi}^{(k)}, v_i)); \end{aligned} \quad (9)$$

where $S_{xe,l}$, $S_{xp,l}$, $S_{v,l}$, and $S_{w,l}$ represent column j of S_{xe} , S_{xp} , S_v , and S_w , respectively. x_{i-1} is the estimation system state, and x_{pi} is the prediction system state at i . m_x represents the dimension of the state vector. m_v represents the dimension of the measurement noise vector. λ represents the given step size, $\lambda^2 = 3$. $A = / (2\lambda)$. $B = (\lambda^2 - 1)^{0.5} / (2\lambda^2)$.

2. Forecast: The one-step predictions $x_{pi}(k)$ can be calculated using the following formula:

$$\begin{aligned}
x_{pi}(k) &= \beta \sum_{p=1}^{m_x} [f_k(x_{i-1}, \omega_{i-1} + \lambda S_{v,l}) + f_k(x_{i-1}, \omega_{i-1} - \lambda S_{v,l})] \\
&+ \beta \sum_{p=1}^{m_w} [f_k(x_{i-1} + \lambda S_{se,l}, \omega_{i-1}) + f_k(x_{i-1} - \lambda S_{se,l}, \omega_{i-1})] + ((\lambda^2 - m_x - m_w) / \lambda^2) f_k(x_{i-1}, \omega_{i-1})
\end{aligned} \quad (10)$$

The compound matrix $S_{xp}^{(k)}(i)$ is obtained using QR decomposition.

$$\begin{aligned}
S_{xp}^{(k)}(i) &= [(S_{xx}^{(1)}(i))^{(k)} (S_{xv}^{(1)}(i))^{(k)} (S_{xx}^{(2)}(i))^{(k)} (S_{xv}^{(2)}(i))^{(k)}], \\
[Q, R] &= qr(S_{xp}^{(k)}(i)^T), S_{xp}^{(k)}(i) = R.
\end{aligned} \quad (11)$$

The covariance matrix $P_{pc}^{(k)}$ can be updated using Equation (12).

$$P_{pc}^{(k)} = S_{xp}^{(k)}(i) S_{xp}^{(k)}(i)^T \quad (12)$$

Similar to $S_{xp}^{(k)}(i)$, the matrix $S_{yp}^{(k)}(i)$ is

$$\begin{aligned}
S_{yp}^{(k)}(i) &= [(S_{yxx}^{(1)}(i))^{(k)} (S_{yvw}^{(1)}(i))^{(k)} (S_{yxx}^{(2)}(i))^{(k)} (S_{yvw}^{(2)}(i))^{(k)}], \\
[Q, R] &= qr(S_{yp}^{(k)}(i)^T), S_{yp}^{(k)}(i) = R.
\end{aligned} \quad (13)$$

Step 3: Update: The predictive capacity y_{pi} is calculated using the following formula:

$$\begin{aligned}
y_{pi}^{(k)} &= \beta \sum_{p=1}^{m_x} [h_k(x_{pi} + \lambda S_{xp,l}, v_i) + h_k(x_{pi} - \lambda S_{xp,l}, v_i)] \\
&+ \beta \sum_{p=1}^{m_w} [h_k(x_{pi}, v_i + \lambda S_{w,l}) - h_k(x_{pi}, v_i - \lambda S_{w,l})] + ((\lambda^2 - m_x - m_w) / \lambda^2) h_k(x_{pi}, v_i)
\end{aligned} \quad (14)$$

The matrix $P_{xy}(i)$ and the gain K_i can be obtained:

$$\begin{aligned}
P_{xy}^{(k)}(i) &= S_{xp}^{(k)}(i) [(S_{yxx}^{(1)}(i))^{(k)}]^{(k)T} \\
K_i^{(k)} &= P_{xy}^{(k)}(i) [S_{yp}^{(k)}(i) S_{yp}^{(k)}(i)^T]^{-1}
\end{aligned} \quad (15)$$

The state estimation $x_i^{(k)}$ is updated:

$$x_i^{(k)} = x_{pi}^{(k)} + K_i^{(k)}(y_i - y_{pi}^{(k)}) \quad (16)$$

where y_i is the terminal voltage of the battery model at i .

The Cholesky factor $S_{xe}^{(k)}(i)$ is obtained in the same way as $S_{xp}^{(k)}(i)$ and $S_{yp}^{(k)}(i)$:

$$\begin{aligned}
S_{xe}^{(k)}(i) &= [S_{xp}^{(k)}(i) - K_i^{(k)}(S_{yxx}^{(1)}(i))^{(k)} K_i^{(k)}(S_{yvw}^{(1)}(i))^{(k)} K_i^{(k)}(S_{yxx}^{(2)}(i))^{(k)} \\
&K_i^{(k)}(S_{yvw}^{(2)}(i))^{(k)}], [Q, R] = qr(S_{xe}^{(k)}(i)^T); S_{xe}^{(k)}(i) = R
\end{aligned} \quad (17)$$

The covariance estimation $P_{ec}^{(k)}$ is updated using Equation (18):

$$P_{ec}^{(k)} = S_{xe}^{(k)}(i) S_{xe}^{(k)}(i)^T \quad (18)$$

The state estimation $x_i^{(k)}$ used in importance sampling can be obtained from Equation (19).

$$x_i^{(k)} \sim N(x_i^{(k)}; P_{ec}^{(k)}) \quad (19)$$

Figure 2 shows a flowchart of the proposed method.

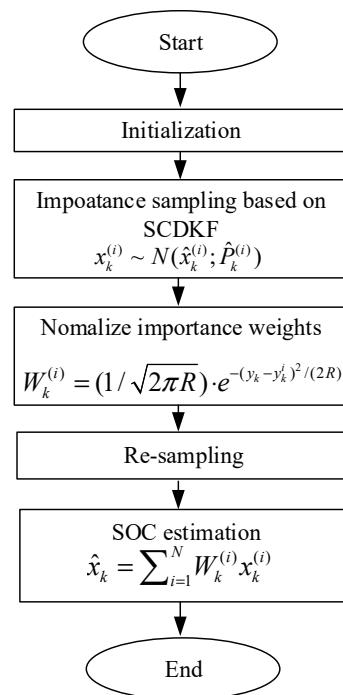


Figure 2. Flowchart of the SCDPF algorithm.

4. Experiment and Simulation Analysis

The ternary 21700 from Lishen battery Co., Ltd., Suzhou, China, with a rated capacity of 4.8 Ah and a rated voltage of 3.6 V, was applied for model parameterization and SOC estimation. This kind of battery has been widely used in many fields such as new energy vehicles, power tools, and so on because it has a high energy density, low cost, and is lightweight. As shown in Figure 3, the experimental platform consisted of a lithium-ion battery charge and discharge test system, a constant temperature chamber, an upper computer, and lithium-ion batteries. The temperature range of the high and low temperature test box was $-40\text{ }^{\circ}\text{C}\sim 150\text{ }^{\circ}\text{C}$. The current acquisition accuracy was 0.001 A, and the voltage acquisition accuracy was 1 mV. The highest frequency of data acquisition was 50 Hz, the interval of data acquisition was 1 s; it supports CAN bus communication, and has many controllable modes, including constant voltage charging, constant current charging, constant current constant voltage charging, pulse charging and discharging, programmable power control, and dynamic condition simulation.

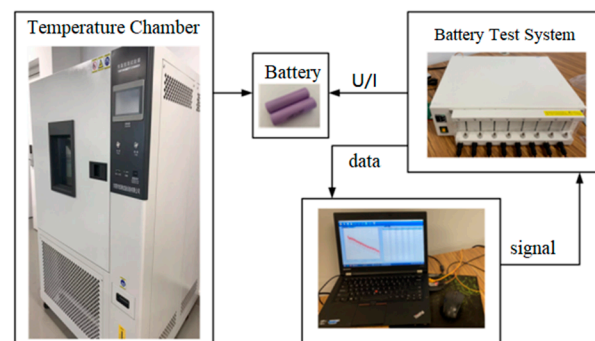


Figure 3. Battery experimental platform.

The capacity and open circuit voltage (OCV) test, HPPC test, and NEDC test were conducted at 25 and $0\text{ }^{\circ}\text{C}$ on the battery experiment platform to collect data about the battery's voltage, current, and temperature.

Fitting the relationship between U_{ocv} and SOC with fifth-order polynomial function can be expressed as follows:

$$\begin{aligned} U_{25} &= 3.7 \times SOC^5 - 12.5 \times SOC^4 + 16.0 \times SOC^3 - 9.6 \times SOC^2 + 3.7 \times SOC + 3.0 \\ U_0 &= 0.6 \times SOC^5 - 3.9 \times SOC^4 + 7.0 \times SOC^3 - 5.3 \times SOC^2 + 2.7 \times SOC + 3.1 \end{aligned} \quad (20)$$

Figure 4 shows the fitting curve.

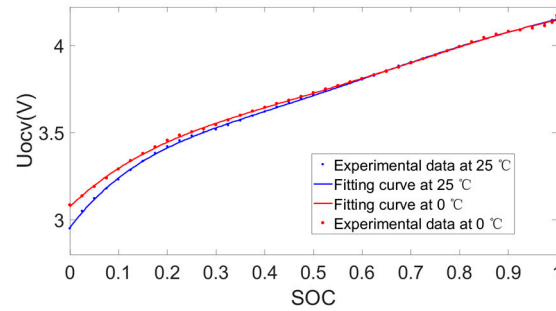


Figure 4. Fitting curve of SOC-OCV.

The HPPC and NEDC tests for identifying the battery model parameters and estimating the SOC of the battery are shown in Figure 5.

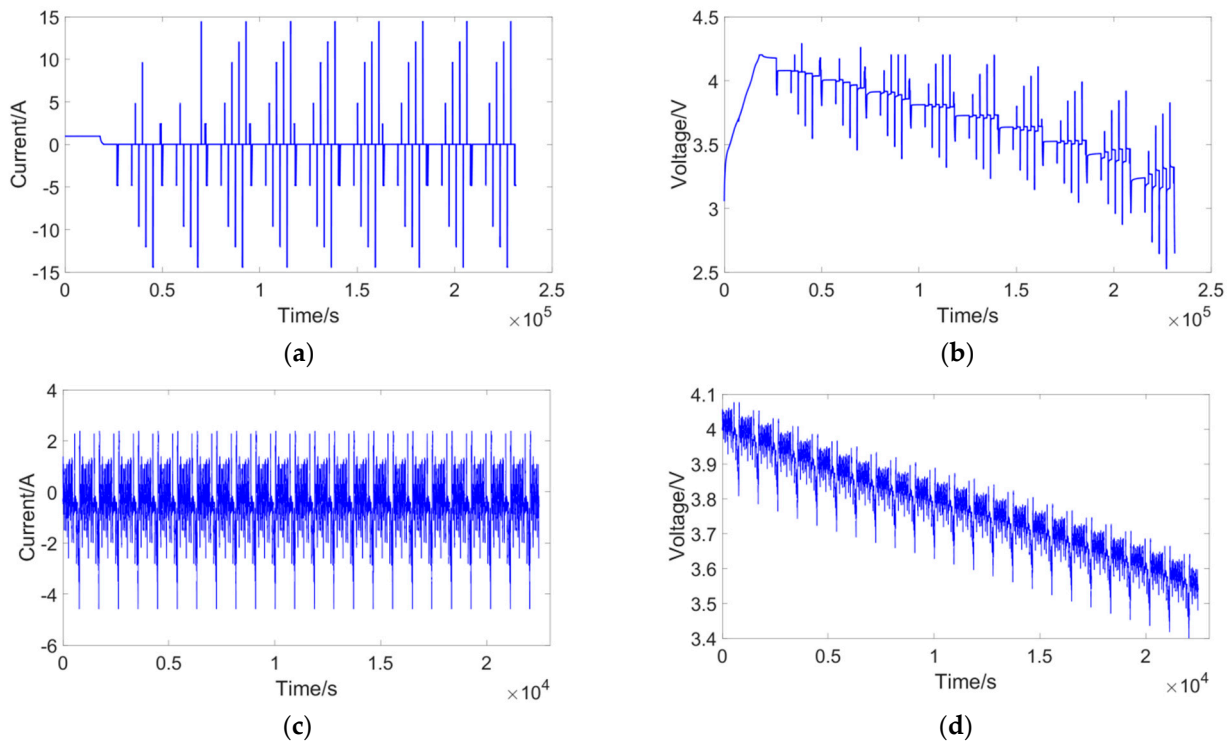


Figure 5. (a) Current in HPPC test; (b) voltage in HPPC test; (c) current in NEDC condition test; (d) voltage in NEDC condition test.

To demonstrate the accuracy and stability of the SOC estimation method, three evaluation criteria were utilized: mean absolute error (MAE), root mean square error (RMSE), and mean absolute percentage error (MAPE).

$$\begin{aligned}
 MAE &= \frac{1}{M} \sum_{n=1}^M |y_n^* - y_n| \\
 RMSE &= \sqrt{\frac{1}{M} \sum_{n=1}^M (y_n^* - y_n)^2} \\
 MAPE &= \frac{1}{M} \sum_{n=1}^M \left| \frac{y_n^* - y_n}{y_n} \right| \times 100\%
 \end{aligned} \tag{21}$$

4.1. Parameter Identification

The parameters of the battery model can be identified using the voltage and current data obtained from the HPPC test. The parameter identification method used was FFRLS, as described in Section 2.2. The model parameters are shown in Table 1. The unit of resistance is mΩ, and the unit of capacitance is F.

Table 1. Battery model parameter identification results.

SOC	R_{ac} (0 °C/5 °C)	R_{ct} (0 °C/5 °C)	R_{wb} (0 °C/5 °C)	C_{ct} (0 °C/5 °C)	C_{wb} (0 °C/5 °C)
0.1	(55.3/30.2)	(4/1)	(18.3/12.1)	(109.1/594.8)	(4989.2/1824.9)
0.2	(51.4/26.9)	(3.69/0.77)	(11.9/8.6)	(188.6/796.2)	(6232.4/2185.2)
0.3	(47.8/25.9)	(3.71/1.2)	(9.2/3.9)	(175.3/465.7)	(9358.4/3040.5)
0.4	(46.9/26.2)	(3.75/0.87)	(9.5/3.9)	(160.5/711)	(7201.9/2385.3)
0.5	(45.6/26.5)	(5.21/0.76)	(9.7/4)	(98.1/818.4)	(6340.5/2042.7)
0.6	(46.3/26.1)	(3.78/0.84)	(11.1/4.5)	(181.3/719.6)	(6430.2/2677.3)
0.7	(49.6/25.1)	(3.8/1.2)	(8.8/39.5)	(190.4/489.1)	(8000/4551.5)
0.8	(42.7/24.6)	(6.1/2.4)	(11.6/15.3)	(61.2/219)	(3580.2/6131.2)
0.9	(47.8/25.7)	(3.2/2.1)	(9.1/2.9)	(185.3/286.1)	(5980/12045)

4.2. Algorithm Simulation Analysis of Accuracy and Convergence

Figure 6 shows the results of the SOC estimation algorithms at 25 °C in comparison with the EKF [50], the UKF [51], the UPF [52], and the proposed SCDPF algorithm during NEDC test. The evaluation criteria used in the the SCDPF SOC estimation method are the smallest error and that the maximum error never exceeds 1.26. Therefore, the SOC estimation has a stronger tracking ability and higher accuracy.

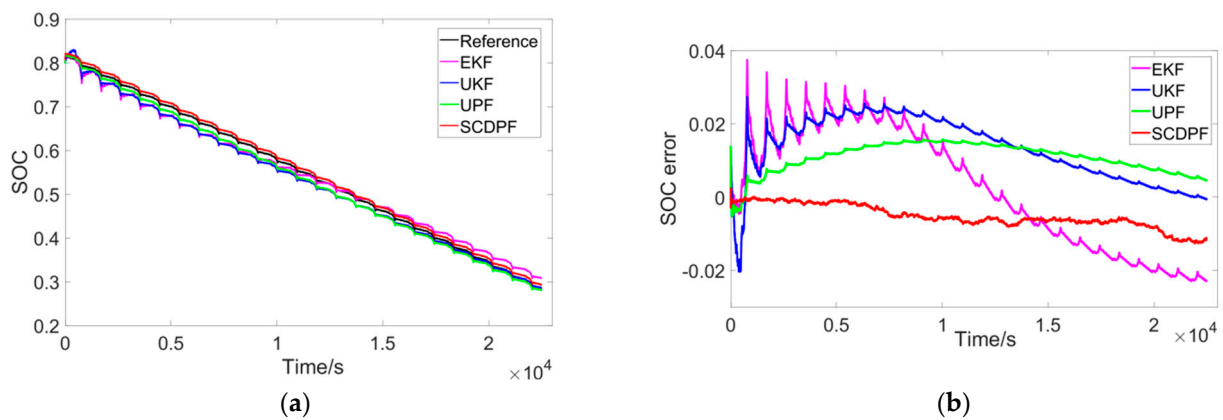


Figure 6. SOC estimation at 25 °C (a) estimated value; (b) estimated error.

Table 2 shows the errors of the SOC estimation algorithms at 25 °C. The SCDPF algorithm achieves a good performance with MAE = 0.0053, RMSE = 0.0061, and MAPE = 0.752%. The SOC errors of MAE, RMSE, and MAPE obtained by EKF are 0.0152, 0.0169, and 2.614%,

respectively. The corresponding SOC errors obtained by UKF are 0.0134, 0.0156, and 2.571%. The corresponding SOC errors obtained by UPF are 0.0109, 0.0115, and 1.856%. The estimation accuracy of the proposed SCDPF algorithm has been significantly improved.

Table 2. SOC estimation errors at 25 °C.

Algorithms	MAE	RMSE	MAPE
EKF (50)	0.0152	0.0169	2.614%
UKF (51)	0.0134	0.0156	2.571%
UPF (52)	0.0109	0.0115	1.856%
SCDPF	0.0053	0.0061	0.752%

Four algorithms were used to estimate the battery SOC at 0 °C and compare with the reference value of SOC. The results are shown in Figure 7. Table 3 shows the errors of SOC estimation algorithms at 0 °C.

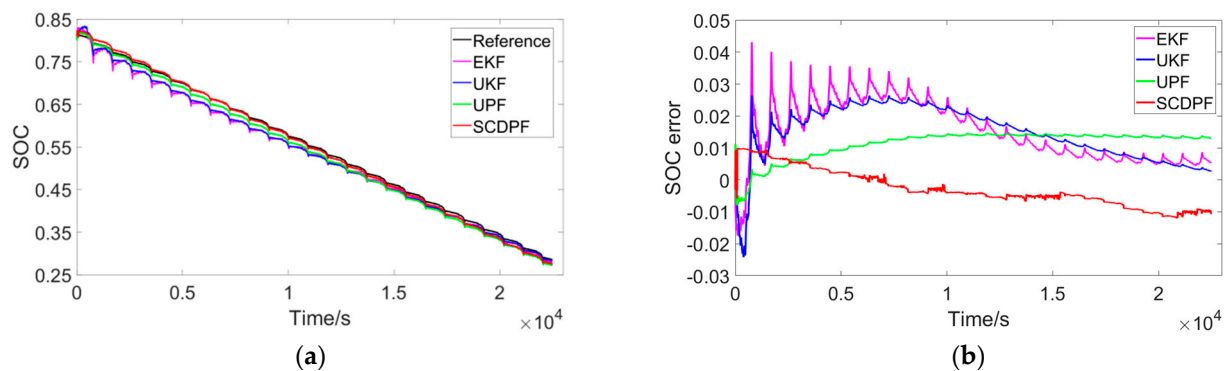


Figure 7. SOC estimation at 0 °C (a) estimated value; (b) estimated error.

Table 3. SOC estimation errors at 0 °C.

Algorithms	MAE	RMSE	MAPE
EKF (50)	0.0157	0.0179	2.939%
UKF (51)	0.0155	0.0170	2.831%
UPF (52)	0.0116	0.0122	1.841%
SCDPF	0.0056	0.0063	0.882%

The figure and table show that the situation at 0 °C is similar to that at 25 °C. The SCDPF algorithm achieves a good performance with MAE = 0.0056, RMSE = 0.0063, and MAPE = 0.782%. The SOC errors of MAE, RMSE, and MAPE obtained by EKF are 0.0157, 0.0179, and 2.939%, respectively. The corresponding SOC errors obtained by UKF are 0.0155, 0.0170, and 2.831%. The corresponding SOC errors obtained by UPF are 0.0116, 0.0122, and 1.841%. The proposed SCDPF algorithm has the minimum estimation error, and the accuracy has clearly been improved.

Convergence analyses of the different SOC estimation algorithms were conducted at the initial SOC values of 0.6 at 25 °C. The SOC values estimated by the four algorithms can quickly converge to the reference, as shown in Figure 8. The convergence rate of the SCDPF algorithm is faster than the three methods with a convergence time of 2 s. Figure 8b shows that the contrast of four algorithms is universal at the initial SOC of 0.6. The tracking trend of the SOC values is the same as that at the initial SOC of 0.8. The SOC estimation error obtained by the SCDPF algorithm varies slightly compared with that at the initial SOC of 0.8, which proves that the stability of the proposed algorithm is relatively higher.

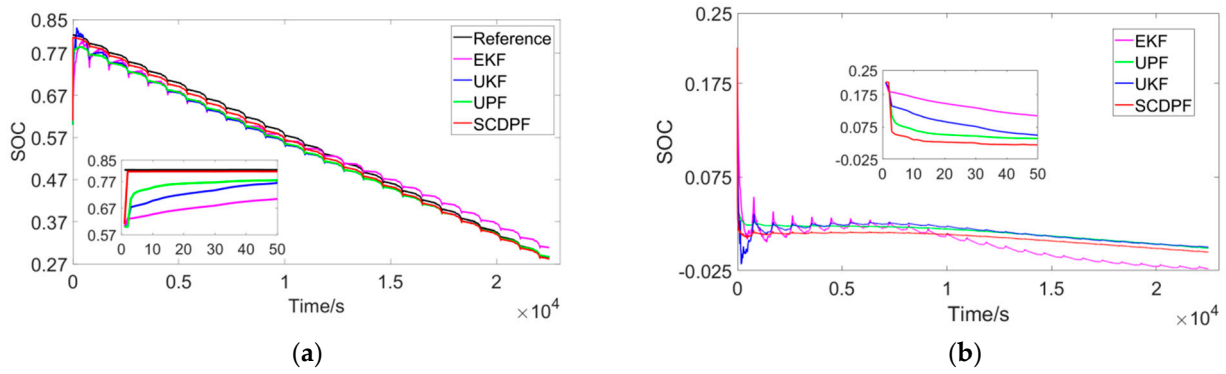


Figure 8. Comparison with an initial SOC of 0.6 (a) estimated value; (b) estimated error.

Table 4 illustrates the SOC estimation errors using the NEDC driving cycle from other studies. Due to varying evaluation criteria, only the RMSE is listed here. These studies also represent improvements to filtering algorithms. In comparison to the method proposed in this paper, although the computational time of SCDPF did not exhibit a significant decrease, our approach markedly enhances the accuracy of SOC estimation.

Table 4. The estimation error of SOC using the NEDC driving cycle from other studies.

Algorithms	RMSE
[53]	0.94%
[54]	0.79%

4.3. Algorithm Simulation Analysis of Robustness

The voltage and current signals of the battery need to be collected through the sensor for SOC estimation as they represent the response and excitation. The measurement deviation caused by the sensor signal is mainly related to the fixed component voltage and current signal offset and the signal transmission crosstalk noise. Gaussian and non-Gaussian noise were added to the measured signal at the initial SOC of 0.8 at 25 °C to verify the robustness of the proposed algorithm in practical application.

Given the presence Gaussian white noise with a mean value of 0 and a standard deviation of 0.02, the calculation formula is as follows:

$$Noise_1 = \alpha_{Noise1} \cdot randn(1, n) \quad (22)$$

where α_{Noise1} is the standard deviation coefficient with the value of 0.02, and n is the length of the predicted data.

$Noise_2$ is a uniformly distributed random noise between [0 and 0.01]. $Noise_3$ is a non-Gaussian white noise superimposed by $Noise_1$ and $Noise_2$, and the calculation formula is as follows:

$$Noise_3 = Noise_1 + \alpha_{Noise2} \cdot rand(1, n) \quad (23)$$

where α_{Noise2} is the uniformly distributed noise coefficient with a value of 0.01.

Adding noise to the current is marked as Case1, while adding noise to the voltage is marked as Case2. Table 5 shows the results of SOC estimation in the case of adding Gaussian and non-Gaussian noise. As shown in the table, after the two kinds of noise are added to the measurement signal, the MAEs of the SOC estimations obtained by SCDPF are 0.877% and 0.976% higher than that obtained by EKF algorithm with Noise1 and Noise3, respectively, under Case1. The MAEs of the SOC estimations obtained by SCDPF are 1.109% and 2.626% higher than that obtained by EKF algorithm with Noise1 and Noise3, respectively, under Case2. The comparison indicates that the SOC estimation result obtained using the SCDPF algorithm is less affected by noise and has a better robustness than that obtained using EKF,

especially in the case of non-Gaussian noise. Similar conclusions can be obtained from the SOC estimation results obtained from SCDPF, UKF, and UPF.

Table 5. Results of SOC estimation under different noise conditions.

SOC Estimation Algorithm		Error	Noise 1	Noise 3
EKF	Case1	MAE (%)	1.5339	1.6817
		RMSE (%)	1.6999	1.8448
	Case2	MAE (%)	2.1102	3.7297
		RMSE (%)	2.615	4.1243
UKF	Case1	MAE (%)	1.4181	1.6922
		RMSE (%)	1.6561	1.8434
	Case2	MAE (%)	1.7935	2.712
		RMSE (%)	1.9762	2.8421
UPF	Case1	MAE (%)	1.2729	1.3698
		RMSE (%)	1.3169	1.4349
	Case2	MAE (%)	1.6600	2.1154
		RMSE (%)	1.7049	2.0803
SCDPF	Case1	MAE (%)	0.65687	0.70558
		RMSE (%)	0.74745	0.76395
	Case2	MAE (%)	1.0007	1.104
		RMSE (%)	1.0489	1.1954

5. Conclusions

This study proposes an SCDPF-based SOC estimation algorithm to improve the accuracy and robustness of SOC estimation. The FFRLS algorithm is employed to identify the parameters of the second-order RC equivalent circuit.

The main contributions are summarized as follows. (1) An SCDKF was used as an important density function to generate optimized particles to overcome the particle degeneracy problem of the PF method. (2) Tests with the proposed algorithm were performed and compared with other estimation methods under NEDC conditions at 25 and 0 °C. (3) The SOC estimates with Gaussian and non-Gaussian noise were compared to discuss the robustness of the proposed algorithm.

The comparison shows that the SCDPF algorithm is superior in terms of accuracy. A comparison of the convergence rate of the SOC estimation at the initial SOC value of 0.6 confirms the stability of the SCDPF algorithm. A comparison of the SOC estimation in the case of adding Gaussian and non-Gaussian noise verifies that the proposed algorithm is less affected by noise and has a better robustness. The SCDPF algorithm represents a novel approach to enhancing SOC estimation in lithium-ion batteries, overcoming the limitations of traditional methods. Its implementation in battery management systems can significantly improve the accuracy of assessing the remaining available capacity, thereby enhancing the overall performance and lifespan of lithium-ion batteries. This advancement is crucial for various applications, including electric vehicles, energy storage systems, and portable electronic devices, where accurate SOC estimation is essential for optimal battery utilization and management.

Author Contributions: Conceptualization, Y.C.; Methodology, Y.C.; Software, Y.C.; Validation, X.H.; Formal analysis, Y.C. and X.H.; Investigation, Y.C.; Writing—original draft, Y.C.; Writing—review and editing, X.H.; Visualization, Y.C. and X.H.; Project administration, Y.C. All authors have read and agreed to the published version of the manuscript.

Funding: This research was funded by the National Natural Science Foundation of China (Grant number 51577046), the State Key Program of the National Natural Science Foundation of China (Grant number 51637004), and the National Key Research and Development Plan “Important Scientific Instruments and Equipment Development” (Grant number 2016YFF0102200).

Data Availability Statement: The original contributions presented in the study are included in the article, further inquiries can be directed to the corresponding author.

Conflicts of Interest: The authors declare no conflicts of interest.

References

1. Li, X.; Yuan, C.; Wang, Z.; Xie, J. A data-fusion framework for lithium battery health condition Estimation Based on differential thermal voltammetry. *Energy* **2022**, *239*, 122206. [[CrossRef](#)]
2. Wang, D.; Kong, J.Z.; Yang, F.; Zhao, Y.; Tsui, K.L. Battery prognostics at different operating conditions. *Measurement* **2020**, *151*, 107182. [[CrossRef](#)]
3. Yang, B.; Wang, J.; Cao, P.; Zhu, T.; Shu, H.; Chen, J.; Zhang, J.; Zhu, J. Classification, summarization and perspectives on state-of-charge estimation of lithium-ion batteries used in electric vehicles: A critical comprehensive survey. *J. Energy Storage* **2021**, *39*, 102572. [[CrossRef](#)]
4. Yu, K.; Wang, H.; Mao, L.; He, Q.; Wu, Q. IC Curve-Based Lithium-Ion Battery SOC Estimation at High Rate Charging Current. *IEEE Trans. Instrum. Meas.* **2022**, *71*, 3160554. [[CrossRef](#)]
5. Ren, Z.; Du, C.; Wu, Z.; Shao, J.; Deng, W. A comparative study of the influence of different open circuit voltage tests on model-based state of charge estimation for lithium-ion batteries. *Int. J. Energy Res.* **2021**, *45*, 13692–13711. [[CrossRef](#)]
6. Liu, Z.; Li, Z.; Zhang, J.; Su, L.; Ge, H. Accurate and Efficient Estimation of Lithium-Ion Battery State of Charge with Alternate Adaptive Extended Kalman Filter and Ampere-Hour Counting Methods. *Energies* **2019**, *12*, 757. [[CrossRef](#)]
7. Lai, X.; Wang, S.; Ma, S.; Xie, J.; Zheng, Y. Parameter sensitivity analysis and simplification of equivalent circuit model for the state of charge of lithium-ion batteries. *Electrochim. Acta* **2020**, *330*, 135239. [[CrossRef](#)]
8. Lai, X.; Wang, S.; He, L.; Zhou, L.; Zheng, Y. A hybrid state-of-charge estimation method based on credible increment for electric vehicle applications with large sensor and model errors. *J. Energy Storage* **2020**, *27*, 101106. [[CrossRef](#)]
9. Xiong, R.; Tian, J.; Shen, W.; Sun, F. A Novel Fractional Order Model for State of Charge Estimation in Lithium-ion Batteries. *IEEE Trans. Veh. Technol.* **2019**, *68*, 4130–4139. [[CrossRef](#)]
10. Pang, H.; Mou, L.J.; Guo, L. Parameter identification and state-of-charge estimation approach for enhanced lithium-ion battery equivalent circuit model considering influence of ambient temperatures. *Chin. Phys. B* **2019**, *28*, 108021. [[CrossRef](#)]
11. Nguyen, T.T.; Khan, A.B.; Ko, Y.; Choi, W. An Accurate State of Charge Estimation Method for Lithium Iron Phosphate Battery Using a Combination of an Unscented Kalman Filter and a Particle Filter. *Energies* **2020**, *13*, 4536. [[CrossRef](#)]
12. Xu, W.; Xu, J.; Yan, X. Lithium-ion battery state of charge and parameters joint estimation using cubature Kalman filter and particle filter. *J. Power Electron.* **2020**, *20*, 292–307. [[CrossRef](#)]
13. Yu, J. State-of-Health Monitoring and Prediction of Lithium-Ion Battery Using Probabilistic Indication and State-Space Model. *IEEE Trans. Instrum. Meas.* **2015**, *64*, 2937–2949. [[CrossRef](#)]
14. Zheng, L.; Zhu, J.; Wang, G.; Lu, D.D.C.; He, T. Differential voltage analysis based state of charge estimation methods for lithium-ion batteries using extended Kalman filter and particle filter. *Energy* **2018**, *158*, 1028–1037. [[CrossRef](#)]
15. Feng, F.; Teng, S.; Liu, K.; Xie, J.; Xie, Y.; Liu, B.; Li, K. Co-estimation of lithium-ion battery state of charge and state of temperature based on a hybrid electrochemical-thermal-neural-network model. *J. Power Sources* **2020**, *455*, 227935. [[CrossRef](#)]
16. Stiasny, J.; Misyris, G.S.; Chatzivasileiadis, S. Physics-Informed Neural Networks for Non-linear System Identification for Power 78 System Dynamics. In Proceedings of the 2021 IEEE Madrid Powertech, Madrid, Spain, 28 June–2 July 2021. [[CrossRef](#)]
17. Cheng, G.; Wang, X.; He, Y. Remaining useful life and state of health prediction for lithium batteries based on empirical mode decomposition and a long and short memory neural network. *Energy* **2021**, *232*, 121022. [[CrossRef](#)]
18. Song, Q.; Wang, S.; Xu, W.; Shao, Y.; Fernandez, C. A Novel Joint Support Vector Machine—Cubature Kalman Filtering Method for Adaptive State of Charge Prediction of Lithium-Ion Batteries. *Int. J. Electroch. Sci.* **2021**, *16*, 210823. [[CrossRef](#)]
19. Song, Y.; Liu, D.; Liao, H.; Peng, Y. A hybrid statistical data-driven method for on-line joint state estimation of lithium-ion batteries. *Appl. Energy* **2020**, *261*, 114408. [[CrossRef](#)]
20. Li, Y.; Xiong, B.; Vilathgamuwa, D.M.; Wei, Z.; Xie, C.; Zou, C. Constrained Ensemble Kalman Filter for Distributed Electrochemical State Estimation of Lithium-Ion Batteries. *IEEE Trans. Ind. Inform.* **2021**, *17*, 240–250. [[CrossRef](#)]
21. Li, Y.; Wei, Z.; Xiong, B.; Vilathgamuwa, D.M. Adaptive Ensemble-Based Electrochemical-Thermal Degradation State Estimation of Lithium-Ion Batteries. *IEEE Trans. Ind. Electron.* **2022**, *69*, 6984–6996. [[CrossRef](#)]
22. Sihvo, J.; Roinila, T.; Stroe, D.I. Novel Fitting Algorithm for Parametrization of Equivalent Circuit Model of Li-Ion Battery From Broadband Impedance Measurements. *IEEE Trans. Ind. Electron.* **2021**, *68*, 4916–4926. [[CrossRef](#)]
23. Wang, D.; Li, X.; Wang, J.; Zhang, Q.; Yang, B.; Hao, Z. Lithium-ion battery equivalent model over full-range state of charge based on electrochemical process simplification. *Electrochim. Acta* **2021**, *389*, 138698. [[CrossRef](#)]
24. He, H.; Xiong, R.; Zhang, X.; Sun, F.; Fan, J. State-of-Charge Estimation of the Lithium-Ion Battery Using an Adaptive Extended Kalman Filter Based on an Improved Thevenin Model. *IEEE Trans. Veh. Technol.* **2011**, *60*, 1461–1469. [[CrossRef](#)]
25. Havangi, R. Adaptive robust unscented Kalman filter with recursive least square for state of charge estimation of batteries. *Electr. Eng.* **2022**, *104*, 1001–1017. [[CrossRef](#)]

26. Shateri, N.; Shi, Z.; Auger, D.J.; Fotouhi, A. Lithium-Sulfur Cell State of Charge Estimation Using a Classification Technique. *IEEE Trans. Veh. Technol.* **2021**, *70*, 212–224. [[CrossRef](#)]
27. Meng, B.; Wang, Y.; Mao, J.; Liu, J.; Xu, G.; Dai, J. Using SoC Online Correction Method Based on Parameter Identification to Optimize the Operation Range of Ni-MH Battery for Electric Boat. *Energies* **2018**, *11*, 586. [[CrossRef](#)]
28. Kalogiannis, T.; Hosen, M.S.; Sokkeh, M.A.; Goutam, S.; Jaguemont, J.; Jin, L.; Qiao, G.; Berecibar, M.; Van Mierlo, J. Comparative Study on Parameter Identification Methods for Dual-Polarization Lithium-Ion Equivalent Circuit Model. *Energies* **2019**, *12*, 4031. [[CrossRef](#)]
29. Bian, X.; Wei, Z.; He, J.; Yan, F.; Liu, L. A Two-Step Parameter Optimization Method for Low-Order Model-Based State-of-Charge Estimation. *IEEE Trans. Transp. Electr.* **2021**, *7*, 399–409. [[CrossRef](#)]
30. Pavkovic, D.; Krznar, M.; Komljenovic, A.; Hrgetic, M.; Zorc, D. Dual EKF-Based State and Parameter Estimator for a LiFePO₄ Battery Cell. *J. Power Electron.* **2017**, *17*, 398–410. [[CrossRef](#)]
31. Zhang, G.; Xia, B.; Wang, J. Intelligent state of charge estimation of lithium-ion batteries based on L-M optimized back-propagation neural network. *J. Energy Storage* **2021**, *44*, 103442. [[CrossRef](#)]
32. Lai, X.; Gao, W.; Zheng, Y.; Ouyang, M.; Li, J.; Han, X.; Zhou, L. A comparative study of global optimization methods for parameter identification of different equivalent circuit models for Li-ion batteries. *Electrochim. Acta* **2019**, *295*, 1057–1066. [[CrossRef](#)]
33. Ren, B.; Xie, C.; Sun, X.; Zhang, Q.; Yan, D. Parameter identification of a lithium-ion battery based on the improved recursive least square algorithm. *IET Power Electron.* **2020**, *13*, 2531–2537. [[CrossRef](#)]
34. Kalman, R.E. A New Approach to Linear Filtering and Prediction Problems. *J. Basic Eng.* **1960**, *82D*, 35–45. [[CrossRef](#)]
35. Sunahara, Y.; Yamashita, K. An Approximate Method of State Estimation for Nonlinear Dynamical Systems. *Int. J. Control.* **1970**, *11*, 957–972. [[CrossRef](#)]
36. Merwe, R.; Wan, E. Sigma-Point Kalman Filters for Probabilistic Inference in Dynamic State-Space Models. In Proceedings of the 2003 IEEE International Conference on Acoustics, Speech, and Signal Processing, Hong Kong, China, 1–6 April 2003.
37. Wang, Y.; Cheng, Y.; Xiong, Y.; Yan, Q. Estimation of battery open-circuit voltage and state of charge based on dynamic matrix control-extended Kalman filter algorithm. *J. Energy Storage* **2022**, *52*, 104860. [[CrossRef](#)]
38. Zhou, Z.; Zhang, C. An Extended Kalman Filter Design for State-of-Charge Estimation Based on Variational Approach. *Batteries* **2023**, *9*, 583. [[CrossRef](#)]
39. Maheshwari, A.; Nageswari, S. Real-time state of charge estimation for electric vehicle power batteries using optimized filter. *Energy* **2022**, *254*, 124328. [[CrossRef](#)]
40. Wang, L.; Ma, J.; Zhao, X.; Li, X.; Zhang, K.; Jiao, Z. Adaptive robust unscented Kalman filter-based state-of-charge estimation for lithium-ion batteries with multi-parameter updating. *Electrochim. Acta* **2022**, *426*, 140760. [[CrossRef](#)]
41. Xing, J.; Wu, P. State of Charge Estimation of Lithium-Ion Battery Based on Improved Adaptive Unscented Kalman Filter. *Sustainability* **2021**, *13*, 5046. [[CrossRef](#)]
42. Chen, L.; Wang, S.; Jiang, H.; Fernandez, C.; Zou, C. Decreasing Weight Particle Swarm Optimization Combined with Unscented Particle Filter for the Non-Linear Model for Lithium Battery State of Charge Estimation. *Int. J. Electrochem. Sci.* **2020**, *15*, 10104–10116. [[CrossRef](#)]
43. Zhang, Z.; Huang, W.; Liao, Y.; Song, Z.; Shi, J.; Jiang, X.; Shen, C.; Zhu, Z. Bearing fault diagnosis via generalized logarithmic sparse regularization. *Mech. Syst. Signal Process.* **2022**, *167*, 108576. [[CrossRef](#)]
44. El Mejdoubi, A.; Chaoui, H.; Gualous, H.; Van den Bossche, P.; Omar, N.; Van Mierlo, J. Lithium-Ion Batteries Health Prognosis Considering Aging Conditions. *IEEE Trans. Power Electron.* **2019**, *34*, 6834–6844. [[CrossRef](#)]
45. Xu, W.; Xu, J.; Liu, B.; Liu, J.; Yan, X. A multi-timescale adaptive dual particle filter for state of charge estimation of lithium-ion batteries considering temperature effect. *Energy Sci. Eng.* **2020**, *8*, 2784–2798. [[CrossRef](#)]
46. Dai, J.; Li, X.; Wang, K.; Liang, Y. A novel STSOSLAM algorithm based on strong tracking second order central difference Kalman filter. *Robot. Auton. Syst.* **2019**, *116*, 114–125. [[CrossRef](#)]
47. Hao, X.; Wang, S.; Fan, Y.; Xie, Y.; Fernandez, C. An improved forgetting factor recursive least square and unscented particle filtering algorithm for accurate lithium-ion battery state of charge estimation. *J. Energy Storage* **2023**, *59*, 106478. [[CrossRef](#)]
48. Wang, Q.; Sun, C.; Gu, Y. Research on SOC estimation method of hybrid electric vehicles battery based on the grey wolf optimized particle filter. *Comput. Electr. Eng.* **2023**, *110*, 108907. [[CrossRef](#)]
49. Chen, Y.; He, Y.; Li, Z.; Chen, L.; Zhang, C. Remaining Useful Life Prediction and State of Health Diagnosis of Lithium-Ion Battery Based on Second-Order Central Difference Particle Filter. *IEEE Access* **2020**, *8*, 37305–37313. [[CrossRef](#)]
50. Chen, Z.; Fu, Y.; Mi, C.C. State of Charge Estimation of Lithium-Ion Batteries in Electric Drive Vehicles Using Extended Kalman Filtering. *IEEE Trans. Veh. Technol.* **2013**, *62*, 1020–1030. [[CrossRef](#)]
51. He, W.; Williard, N.; Chen, C.; Pecht, M. State of charge estimation for electric vehicle batteries using unscented Kalman filtering. *Microelectron. Reliab.* **2013**, *53*, 840–847. [[CrossRef](#)]
52. Liu, F.; Ma, J.; Su, W. Unscented Particle Filter for SOC Estimation Algorithm Based on a Dynamic Parameter Identification. *Math. Probl. Eng.* **2019**, *2019*, 1265930. [[CrossRef](#)]

53. Su, L.; Zhou, G.; Hu, D.; Liu, Y.; Zhu, Y. Research on the State of Charge of Lithium-Ion Battery Based on the Fractional Order Model. *Energies* **2021**, *14*, 6307. [[CrossRef](#)]
54. Ye, Y.; Li, Z.; Lin, J.; Wang, X. State-of-charge estimation with adaptive extended Kalman filter and extended stochastic gradient algorithm for lithium-ion batteries. *J. Energy Storage* **2022**, *47*, 103611. [[CrossRef](#)]

Disclaimer/Publisher's Note: The statements, opinions and data contained in all publications are solely those of the individual author(s) and contributor(s) and not of MDPI and/or the editor(s). MDPI and/or the editor(s) disclaim responsibility for any injury to people or property resulting from any ideas, methods, instructions or products referred to in the content.